ENSO Feedback Biases Common to Atmosphere-Ocean Coupled and Atmosphere-Only Simulations of CMIP6 Climate Models

Michiya Hayashi[1]

[1]National Institute for Environmental Studies

March 26, 2023

Abstract

Climate models reproduce sea surface temperature (SST) variability of El Niño/Southern Oscillation (ENSO) despite systematic feedback errors. Atmospheric feedback in response to ENSO's SST anomalies remains biased even in atmosphere-only simulations, but the reason therein is unclear. This study focuses on atmospheric internal processes to reveal ENSO feedback biases common to the atmosphere-ocean coupled historical and atmosphere-only simulations of CMIP6. The net heat flux feedback becomes comparable to observations once the observed SST is prescribed, but the central Pacific zonal wind feedback is yet underestimated albeit a realistic equatorial precipitation-SST relation. The wind feedback bias is attributed to the wind responses to the equatorial precipitation anomalies that seasonally erroneously decline in boreal late winter, common to both the coupled and atmosphere-only simulations. The model's mean state with peak-reduced and broad deep convective areas is favorable for enhancing the wind-precipitation relation and thus ENSO dynamic feedback.

Hosted file

`958824_0_art_file_10811084_rrpgfw.docx` available at https://authorea.com/users/597979/articles/630771-enso-feedback-biases-common-to-atmosphere-ocean-coupled-and-atmosphere-only-simulations-of-cmip6-climate-models

ENSO Feedback Biases Common to Atmosphere-Ocean Coupled and Atmosphere-Only Simulations of CMIP6 Climate Models

M. Hayashi[1]

[1]Earth System Division, National Institute for Environmental Studies, Tsukuba, Japan.

Corresponding author: Michiya Hayashi (hayashi.michiya@nies.go.jp)

Key Points:

- Atmospheric dynamic feedback of ENSO is biased common to the coupled and uncoupled CMIP6 climate model simulations.
- In both simulations, the central Pacific zonal wind response to the equatorial precipitation anomalies is too weak in boreal late winter.
- Simulating a peak-reduced and broad deep convective mean state is favorable for enhancing the wind response and thus dynamic feedback.

Abstract

Climate models reproduce sea surface temperature (SST) variability of El Niño/Southern Oscillation (ENSO) despite systematic feedback errors. Atmospheric feedback in response to ENSO's SST anomalies remains biased even in atmosphere-only simulations, but the reason therein is unclear. This study focuses on atmospheric internal processes to reveal ENSO feedback biases common to the atmosphere-ocean coupled historical and atmosphere-only simulations of CMIP6. The net heat flux feedback becomes comparable to observations once the observed SST is prescribed, but the central Pacific zonal wind feedback is yet underestimated albeit a realistic equatorial precipitation-SST relation. The wind feedback bias is attributed to the wind responses to the equatorial precipitation anomalies that seasonally erroneously decline in boreal late winter, common to both the coupled and atmosphere-only simulations. The model's mean state with peak-reduced and broad deep convective areas is favorable for enhancing the wind-precipitation relation and thus ENSO dynamic feedback.

Plain Language Summary

El Niño/Southern Oscillation (ENSO) is a key tropical Pacific atmosphere-ocean coupled phenomenon for modulating year-to-year climate worldwide, of which sea surface temperature (SST) variability is successfully simulated by the current generation of global climate models. However, atmospheric feedback processes regarding the ENSO growth are systematically too weak primarily due to too cold eastern equatorial Pacific SST in the atmosphere-ocean coupled model simulations, potentially adding uncertainty in seasonal forecasts and future projections. Such feedback bias remains even when observed SSTs drive the atmosphere-only models, but its reason is yet elucidated. This study analyzed the state-of-the-art climate models and observational datasets to reveal what characterizes the too-weak atmospheric feedback common to the coupled and atmosphere-only models. The atmosphere-only models well simulate the equatorial precipitation increase with warm eastern Pacific SST anomalies but systematically underestimate the central Pacific westerly wind response to the increased equatorial precipitation. The wind-precipitation relation erroneously declines in boreal late winter after ENSO becomes matured, irrespective of the model types. To reduce the seasonal wind-precipitation relation bias, the long-term averaged tropical precipitation in climate models needs to have a reduced amplitude in the most convectively active area and be broadened toward convectively suppressed areas.

1 Introduction

El Niño/Southern Oscillation (ENSO) is the dominant interannual mode driven by equatorial Pacific atmosphere-ocean interactions and its large-scale circulation associated with tropical precipitation variability modulates year-to-year climate worldwide (Philander, 1990; Jin, 1997; Timmermann et al., 2018). Most current atmosphere-ocean coupled climate models can produce the observed amplitude of ENSO's sea surface temperature (SST) variability in the equatorial Pacific and its remote teleconnection pattern (Planton et al., 2020; McGregor et al., 2022), but the majority suffer from biased ENSO feedback for decades (Guilyardi et al., 2009, 2020; Kim et al., 2014; Bellenger et al., 2014; Bayr et al., 2020, hereafter BDL20; Hayashi et al., 2020). The atmospheric part of ENSO feedback composes of key two dynamic and thermodynamic processes: the positive zonal wind feedback and negative net heat flux feedback. Both processes tend to be underestimated in climate models so that feedback errors are compensated to each other, resulting in a seemingly realistic ENSO amplitude (Guilyardi et al., 2009; Bayr et al., 2019). Too weak ENSO feedback causes a poor simulation of ENSO asymmetry (Hayashi et al., 2020; Bayr & Latif, 2022), which in turn affects the robustness of future projections of the ENSO amplitude and teleconnections under global warming (Cai et al., 2018, 2021; Bayr & Latif, 2022).

The too-weak ENSO feedbacks in coupled models are connected to too-cold eastern Pacific mean-state SST (excessive cold tongue) that shifts the Pacific Walker circulation to the west (BDL20). The cold tongue bias tends to be reduced by increasing the horizontal resolution of ocean models to better resolve eddy-driven heat transport (Wengel et al., 2021; Liu et al., 2022). In uncoupled atmospheric-only model simulations, where the SST is prescribed by observations, both dynamic and thermodynamic feedbacks are substantially improved from the corresponding coupled simulations, but their strength and related atmospheric circulation response remain too weak (BDL20; Wang et al., 2021). These circulation biases originate from atmospheric models and potentially induce erroneous ENSO dynamics in coupled models as well. However, it remains unclear whether there would be common feedback biases in both the coupled and uncoupled models.

This study analyzes ENSO feedback processes simulated by the state-of-the-art climate models participating in the Coupled Model Intercomparison Project phase 6 (CMIP6, Eyring et al., 2016) by focusing on atmospheric internal processes in atmosphere-ocean coupled and uncoupled simulations. As the atmospheric circulation responses are driven by condensation heating that accompanies precipitation, equatorial Pacific atmospheric responses to ENSO's SST anomalies (SSTAs) are separated into the precipitation response to the SST anomalies and atmospheric responses to the precipitation anomalies. This study further aims to reveal what characterizes the ENSO feedback biases originating from atmospheric models.

2 Data

Monthly outputs from the atmosphere-ocean coupled historical and atmosphere-only (Atmosphere Model Intercomparison Project, AMIP) runs of 32 CMIP6 climate models are analyzed. The historical and AMIP ensembles are composed of the first realizations represented as "r1" (Supplementary Table S1). Each model performance is not focused on since precisely evaluating ENSO feedback requires a large ensemble (Lee et al., 2021). For the observed SST, Centennial in situ Observation-Based Estimates of the Variability of SST and Marine Meteorological Variables version 2 (COBE-SST2, Hirahara et al., 2014) is used. The Global Precipitation Climatology Project version 3.2 (GPCP3, Huffman et al., 2022), Multi-Source Weighted-Ensemble Precipitation version 2.8 (MSWEP28, Beck et al., 2019), and CPC Merged Analysis of Precipitation (CMAP, Xie & Arkin, 1997) datasets are used for the observed precipitation. The atmospheric fields are derived from the fifth-generation ECMWF Reanalysis (ERA5, Hersbach et al., 2019a, 2019b) and the Japanese 55-year Reanalysis (JRA-55, Kobayashi et al. 2015). These datasets available for 1983-2014 are remapped to 2.5°x2.5°. The entire period is used to define climatology.

The Niño-3.4 (170°E-150°W, 5°S-5°N) SSTAs are used to characterize ENSO's SST variability. The zonal wind stress (U) and the zonal winds at the surface and 850 hPa (Us and U850) are averaged in the central Pacific domain (CPac; 150°E-120°W, 5°S-5°N), zonally wider than the Niño-4 region (160°E-150°W, 5°S-5°N) to broadly capture the equatorial wind responses. The vertical velocity at 500 hPa (Ω500) is separately analyzed in the Niño-3 (150°W-

90°W, 5°S-5°N) and Niño-4 regions. The precipitation (P) is averaged in the Niño-3 and Niño-4 combined equatorial Pacific domain (EqPac; 160°E-90°W, 5°S-5°N). The EqPac net surface heat flux (Q) and its surface shortwave (SW) and longwave (LW) radiative, sensible (SH), and latent (LH) heat flux components are also assessed.

3 Results

The simulated ENSO feedbacks are compared with observational values (Fig. 1a). In the historical runs, both the positive dynamic and negative thermodynamic feedbacks, defined as the CPac U and EqPac Q anomalies regressed onto the Niño-3.4 SSTAs, are highly uncertain and too weak in all models (55% and 54% on average relative to the observational means; Supplementary Table S2). As the two feedbacks are correlated among the models (r=-0.52), the underestimated positive feedback is compensated by the underestimated negative feedback. This error compensation is attributable to the cold tongue SST bias (BDL20). In the AMIP runs, both feedbacks are enhanced than the historical runs but still underestimated, as also seen in CMIP5 (BDL20). The ensemble averages of the dynamic and thermodynamic feedbacks are 84% and 90% of observations. Even though the SST is identically provided from observations and thus there is no error compensation between the two feedbacks in the AMIP runs, the intermodel spreads remain substantial. These results suggest that the atmospheric internal processes solely generate the ENSO feedback biases and uncertainties to a large extent.

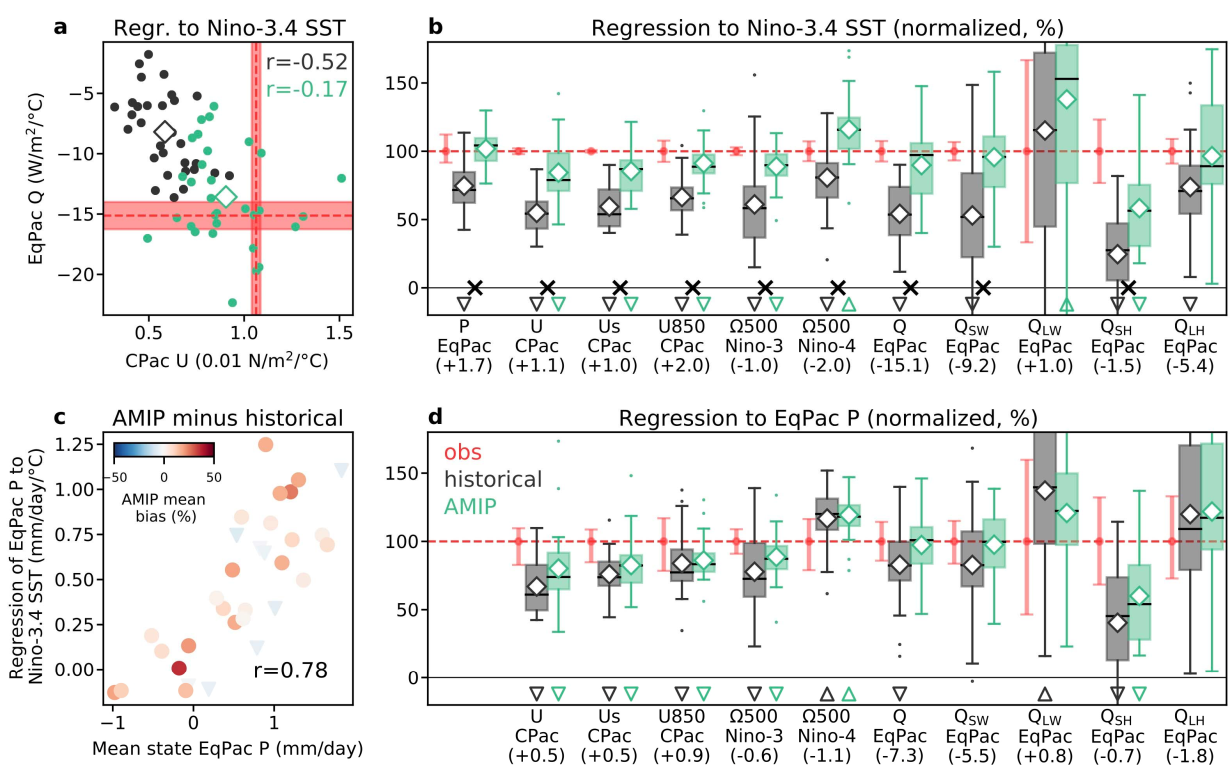

Figure 1. Atmospheric responses to the Niño-3.4 SST and EqPac precipitation anomalies in the historical (black) and AMIP (green) ensembles compared with the observational averages and

min-max ranges (red). (**a**) Scatterplots of the dynamic (x-axis) and thermodynamic (y-axis) feedback coefficients. (**b**) Box-whisker plots of regression coefficients to the Niño-3.4 SSTAs normalized by the observational averages (numbers shown below the x-axis without the units). The up- and down-pointing triangles indicate that the historical and AMIP ensemble means are overestimated and underestimated significantly by the student's t-test and the cross marks represent the ensemble mean differences are significant by Welch's t-test at the 99% confidence levels. (**c**) Changes in the mean-state EqPac P and the P-SST relation from the historical to AMIP runs. Colors represent the mean-state EqPac P bias in the AMIP runs (% relative to the observational average). (**d**) Same as in b but for the regression to the EqPac P anomalies. Diamonds in a, b, and d show the ensemble means.

Various atmospheric responses to the Niño-3.4 SSTAs are examined (Fig. 1b). Here, each response is normalized by the observational average. The EqPac P anomalies regressed onto the Niño-3.4 SSTAs (hereafter, P-SST relation) are too weak in almost all the historical runs (75% on average), but the AMIP runs reproduce it consistent with observations (102%). The difference from the historical to AMIP ensembles is significant at the 99% confidence level, indicating the atmospheric models can reasonably simulate the P-SST relation. Indeed, the increments of the P-SST relation from the historical to AMIP runs are highly correlated with the mean-state EqPac P increments (r=0.78, Fig. 1c). Note that the higher increment of the mean-state precipitation does not correspond to the less biased climatology in the AMIP runs since there is no systematic relation between the increments and the AMIP mean-state biases (Fig. 1c). The dynamic feedback (hereafter, U-SST relation) and related circulation responses are significantly enhanced from the historical to AMIP runs (Fig. 1b). Similarly, the ensemble averages of the CPac Us and U850 responses are respectively changed from 59% and 66% (historical) to 85% and 91% (AMIP). The Niño-3 and Niño-4 Ω500 responses are too weak in the historical runs (61% and 81%) while both are enhanced in the AMIP runs (89% and 116%). Therefore, the circulation responses to the Niño-3.4 SSTAs are too weak even in the AMIP runs, except for the too-strong Niño-4 Ω500 response. Meanwhile, the thermodynamic feedback and each component are significantly enhanced from the historical to AMIP runs, except for the LW and LH responses that have large intermodel uncertainties. In the AMIP runs, the SW and LH responses are close to observations on average. The SH response is too weak, and the LW response tends to be overestimated, but these are minor terms. Thus, the net thermodynamic feedback is not systematically biased once the mean-state SST bias is reduced.

Why the AMIP U-SST relation is systematically underestimated despite that the atmospheric models reasonably reproduce the P-SST relation? As this bias originates from the atmospheric models (Fig. 1b), the same issue may appear in the coupled simulations but potentially hidden behind the dominant mean-state biases. To confirm if this bias is common to the historical and AMIP runs, atmospheric responses to the EqPac P anomalies are examined (Fig. 1d). All the relationships in Fig. 1d are not significantly distinguished between the historical and AMIP runs, differently from Fig. 1b, indicating that their biases are common to both simulations. The CPac U anomalies regressed to the EqPac P anomalies (hereafter, U-P relation) are underestimated as well as the Us and U850 anomalies. On average, the U, Us, and U850 responses in the historical and AMIP runs are 67% and 80%, 76% and 83%, and 84% and 86%, respectively. The Niño-3 Ω500 responses are also too weak (78% and 89% in the historical and AMIP runs, respectively) while the Niño-4 Ω500 responses are too intense (117% and 119%). In contrast, the EqPac Q responses are close to observations on average in the AMIP runs (97%) and not statistically different from those moderately underestimated in the historical runs (83%). Two major components of the EqPac Q response, SW and LH, are not biased while the SH component is underestimated and the LW component is moderately overestimated. As the biased terms are minor, the CMIP6 atmospheric models reasonably reproduce the Q and P relationship. In summary, the common issue for simulating ENSO in the CMIP6 coupled and uncoupled models appears not in the thermodynamic feedback but in the dynamic feedback via the underestimated U-P relation.

The seasonal biases related to the dynamic feedback are further examined in each calendar month (Fig. 2). In observations, the P-SST relation is enhanced in boreal spring (March-April-May, MAM) and suppressed in autumn (September-October-November, SON) and its seasonal difference is as large as the annual estimate (Fig. 2a). The AMIP runs well reproduce its amplitude and seasonal march. The historical runs also simulate a similar seasonality, but the P-SST relation is too weak throughout the year. The observed U-SST relation has two moderate peaks in MAM and SON (Fig. 2b). The MAM peak corresponds to the peak season of the P-SST relation (Fig. 2a). In the historical runs, the U-SST relation is too weak regardless of the seasons. The AMIP runs reproduce the observed amplitude of the U-SST relation from May to November but fail to simulate it from December to April despite that the P-SST relation peaking in MAM is comparable to observations. These results are also confirmed in Us and U850 (Fig. 2c,d). In a similar manner, the seasonal dependence of the U-P relation is analyzed (Fig. 2e-g). The observed amplitude becomes higher in July-December and suppressed in January-June (Fig. 2e). This peak season corresponds to the SON peak of the U-SST relation (Fig. 2b). The seasonally varying U-P relation is almost identical between the historical and AMIP runs and captures the observed values during the peak season (SON). However, the simulated U-P relation is substantially underestimated in boreal late winter (January-February-March, JFM). This bias is also apparent in Us and U850 (Fig. 2f,g). Therefore, the underestimated U-P relation common to the CMIP6 historical and AMIP runs (Fig. 1d) is attributable to the wind response biases in JFM.

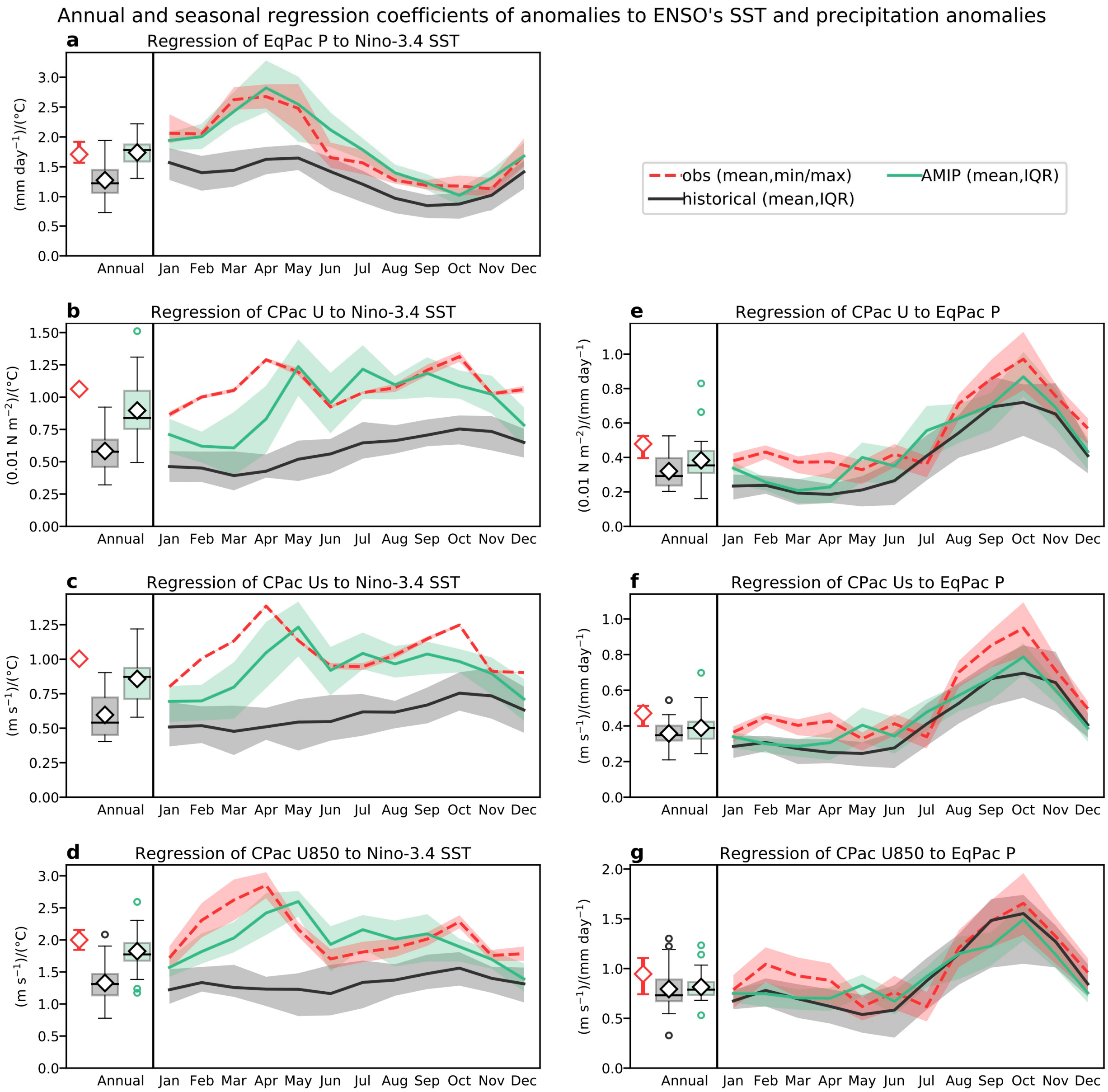

Figure 2. Seasonal dependence of the atmospheric responses to the Niño-3.4 SST and EqPac precipitation anomalies in the historical (black) and AMIP (green) ensembles compared with the observational averages and min-max ranges (red). The regression coefficients of the (**a**) EqPac P, (**b**) CPac U, (**c**) CPac Us, and (**d**) CPac U850 anomalies to the Niño-3.4 SST anomalies. (**e-g**) Same as in b-d but for the regression to the EqPac P anomalies. The lines with shading are the ensemble averages and inter-quartile ranges in each calendar month. The annual plots are as in Fig. 1 but with the units.

The spatial pattern biases of the JFM-averaged zonal wind responses to the EqPac P anomalies are investigated (Fig. 3). In observations (Fig. 3a), the eastward (positive) wind stress response is dominated along the equator, extended from 150°E to 120°W approximately and shifted southward seasonally. The wind stress biases in both runs are significantly negative at the northern and southern sides of the eastward wind responses (Fig. 3 b,c). The zonal-mean wind stress response for 150°E-120°W shows that the simulated response is almost identical between the historical and AMIP runs and is underestimated especially in the southern off-equator (Fig. 3d). Therefore, the central Pacific wind stress responses in the coupled and uncoupled models are too weak and meridionally narrow. Figure 3 also demonstrates the model biases in the tropospheric equatorial zonal wind responses. In both runs (Fig. 3f,g), the simulated wind patterns are overall similar to observations (Fig. 3e), but the negative and positive biases are significant over the central to eastern Pacific in the lower- and upper troposphere, respectively. Despite that the historical runs suffer from the wind responses shifted westward due to the excessive cold tongue (Fig. 3f), the CPac zonal wind response is similarly underestimated through the lower troposphere in both historical and AMIP runs (Fig. 3h).

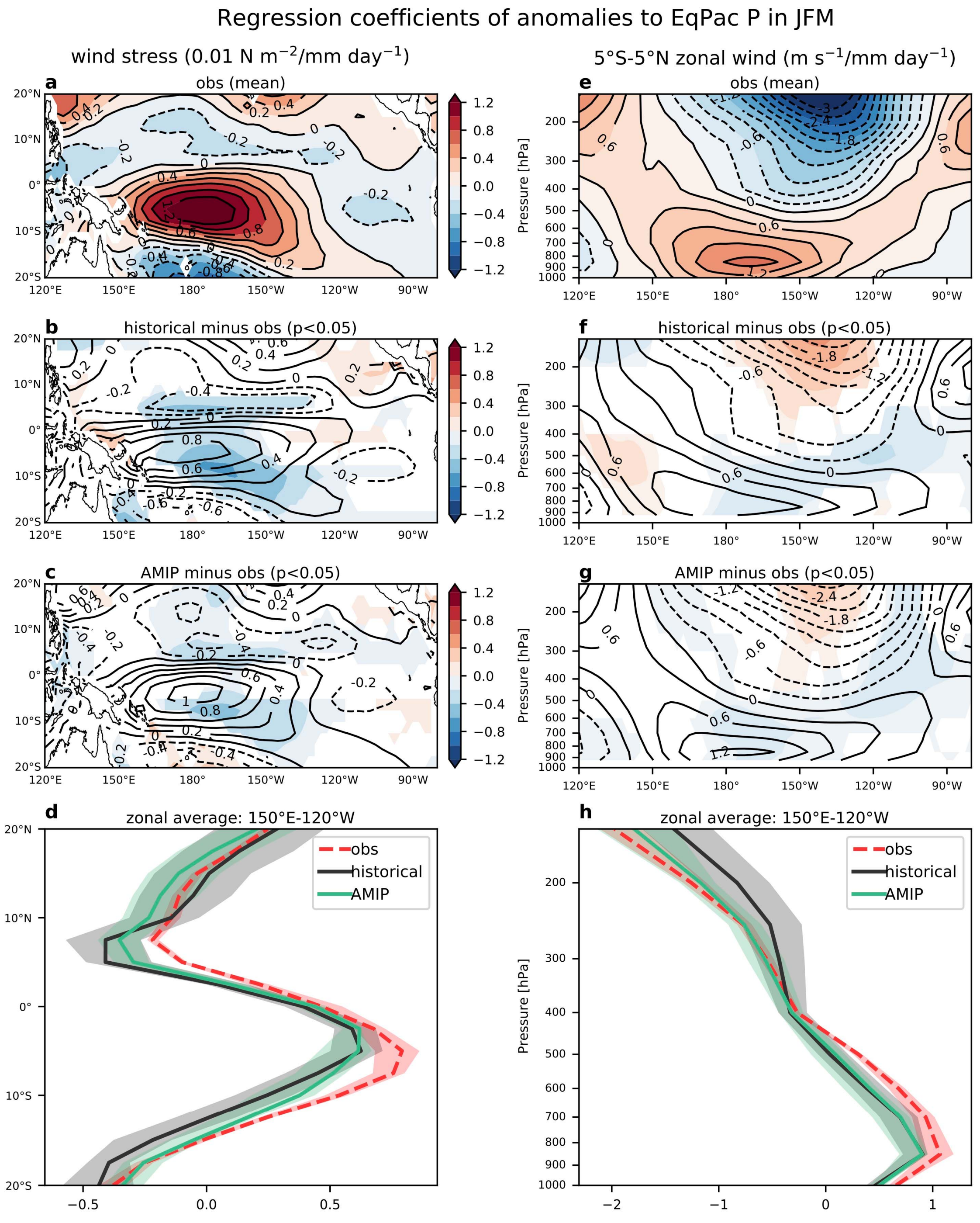

Figure 3. Regressed anomalies of the (left) zonal wind stress and (right) zonal wind between 5°S-5°N to the EqPac precipitation anomalies in JFM. (**a,e**) Observational averages. (**b,c,f,g**) Contours show the ensemble averages and shadings are the model biases relative to the observational averages with p<0.05 by the student's t-test. (**d,h**) Zonal averaged values between 150°E and 120°W. Shown are the observational averages and min-max ranges (red) and the ensemble averages and interquartile ranges of the historical (black) and AMIP (green) runs.

The zonal wind biases in Fig. 3 are related to the P response patterns and equatorial Ω500 response profiles to the EqPac P anomalies (Fig. 4). The anomalous P pattern in JFM shows that the most active (positive) convective response near the dateline is shifted southward in observations (Fig. 4a), accompanied by the southward wind shift (Fig. 3a). In the AMIP runs (Fig. 4c,d), the active convective response over the central Pacific has its peak along the equator on average. Thus, the precipitation response tends to be suppressed in the southern off-equator from 3°S to 10°S to the east of the dateline but too strong near the equator. The equatorially confined precipitation anomalies drive the equatorial ascending (negative Ω500) anomalies too intense in the central Pacific and too weak in the easternmost Pacific (Fig. 4e,g), therefore reducing the lower-tropospheric eastward and upper-tropospheric westward equatorial wind responses (Fig. 3g,h). In the historical runs (Fig. 4b,f), these equatorial P and Ω500 biases are not obvious due to the westward-shifted Walker circulation and also the too-intense climatological South Pacific convergence zone (Brown et al., 2020). Nevertheless, the tropospheric ascending responses are overestimated over the Niño-4 region to a similar extent to the AMIP runs (Fig. 4h) and also suppressed over the easternmost Pacific (Fig. 4f). Furthermore, the suppressed P response east to the dateline in the southern off-equator is significant in the historical runs as well (Fig. 4b,c). These biases are consistent with the reduced lower-tropospheric wind response (Fig. 3b,f).

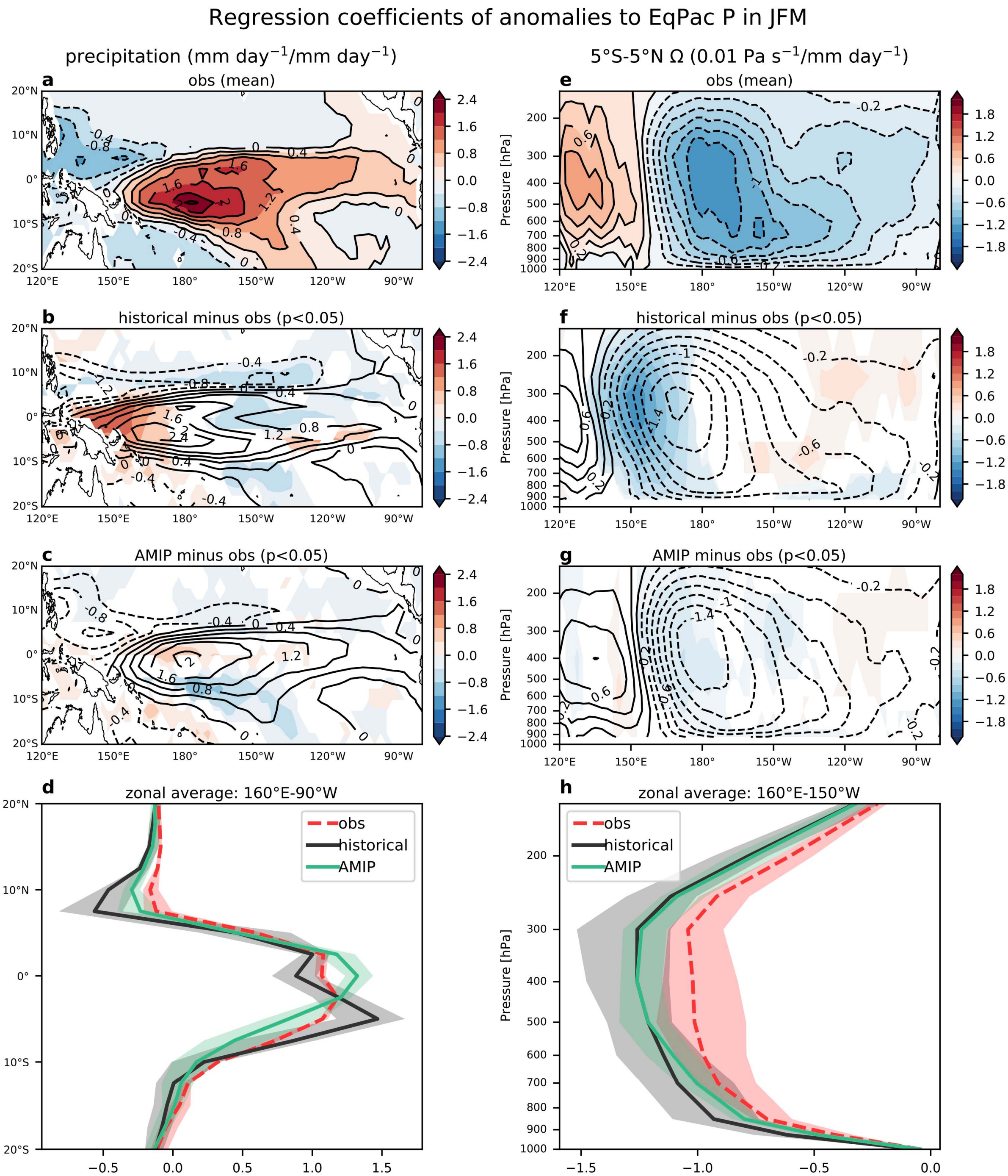

Figure 4. Regressed anomalies of the (left) precipitation and (right) vertical pressure velocity between 5°S-5°N to the EqPac precipitation anomalies in JFM. As in Fig. 3 but for the zonal averaged values between 160°E and 90°W in **d** and between 160°E and 150°W (CPac) in **h**.

What controls the seasonal U-P relation bias in JFM? The intermodel correlation between the U-P relation and the mean-state tropical precipitation in each ensemble is negative over the convectively active warm-pool region in the western Pacific while it is positive over the convectively suppressed off-equatorial areas such as the northwestern and southeastern Pacific (Fig. 5a,c). The AMIP intermodel regression coefficient map of the mean precipitation onto the normalized U-P relation (Fig. 5d) shows that the mean-state precipitation reduced over the warm pool and expanded to the northwestern and southeastern off-equatorial Pacific ("peak-reduced and broad" tropical deep convection) is preferable for enhancing the U-P relation. This peak-reduced and broad pattern is also recognized in the historical runs (Fig. 5a,b), despite their substantially biased mean-state SST and precipitation patterns. These results imply that tuning the model climatology to have less warm-pool precipitation and more descending area precipitation may increase the dynamic feedback.

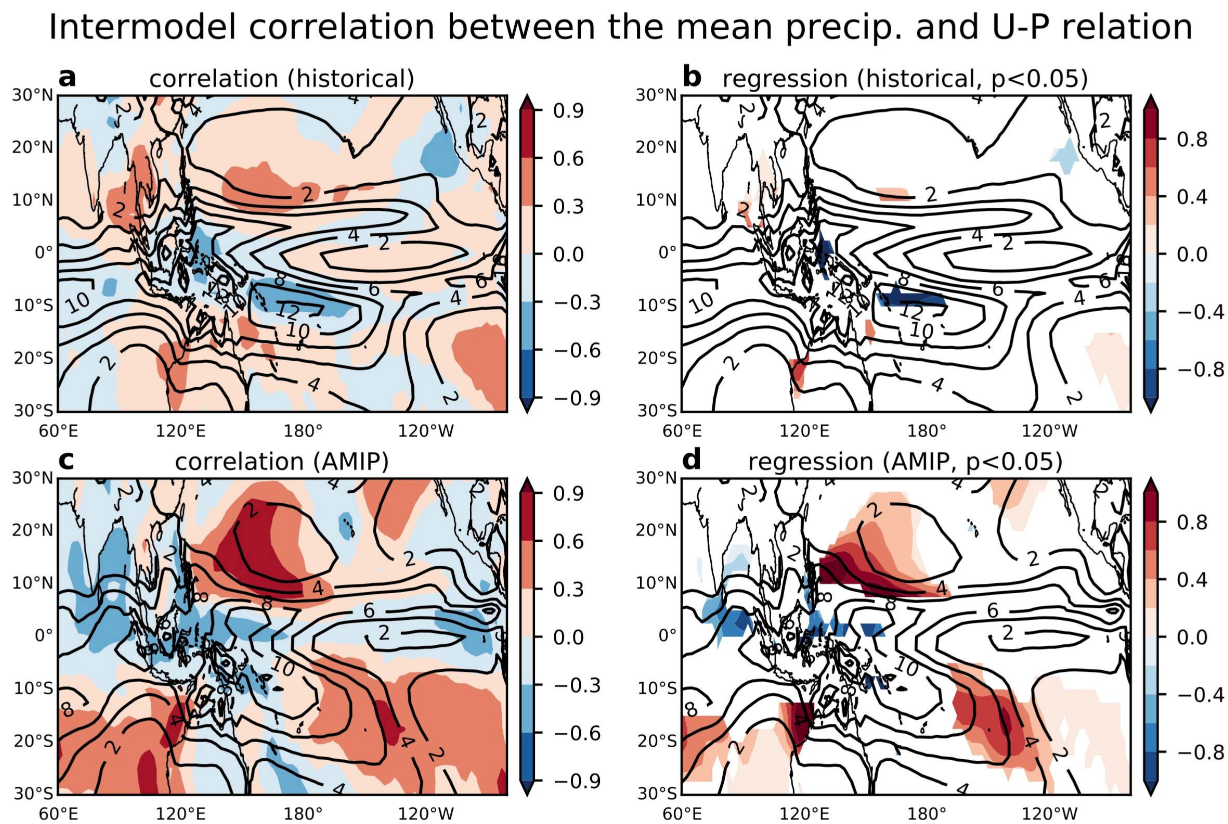

Figure 5. Intermodel (left) correlation and (right) regression coefficients of the mean-state precipitation to the normalized U-P relation in JFM in the (top) historical and (bottom) AMIP runs. The contours indicate the ensemble mean of the mean-state precipitation in the historical and AMIP runs. (b,d) Shadings show the regression coefficients with $p<0.05$.

4 Conclusions and discussion

This study analyzed the coupled historical and uncoupled AMIP simulations of CMIP6 to reveal what characterizes biases in the atmospheric ENSO feedback. Both the positive dynamic and negative thermodynamic feedbacks are underestimated in the CMIP6 historical runs (Planton et al., 2021), but substantially increased in the CMIP6 AMIP runs as the observed SST produces higher mean-state precipitation and thus the equatorial precipitation anomalies in response to ENSO's SST variability (Fig. 1a-c). In the AMIP runs, the thermodynamic feedback becomes comparable to observations as the SW response is improved (Fig. 1b). However, the dynamic feedback represented by the central Pacific zonal wind response remains too weak in the majority of the CMIP6 AMIP runs (Fig. 1b), as in the former generation of climate models in CMIP5 (BDL20), despite that the equatorial precipitation response is not systematically biased. The underestimation of the AMIP dynamic feedback seasonally appears in boreal late winter and is attributed to too-weak zonal wind response to the equatorial precipitation anomalies, common to both the historical and AMIP runs (Figs. 1d and 2). The biased wind-precipitation relation coincides with equatorial ascending anomalies too weak over the eastern Pacific and too strong over the western Pacific and characterized by equatorially confined precipitation anomalies (Figs. 3 and 4). The model mean state with peak-reduced and broad deep convective areas is favorable for enhancing the wind-precipitation relation and thus the dynamic feedback (Fig. 5).

The underestimated dynamic feedback is a long-standing issue since the former generation of climate models. BDL20 found that in CMIP5 AMIP runs, the too-weak wind response to the Niño3.4 SSTAs may be increased by enhancing the Niño-4 Ω500 response, which is already overestimated, as also confirmed in CMIP6 (Figs. 1 and 4). Thus, tuning models to enhance the Ω500 response is not physically reasonable for improving the dynamic feedback. The seasonal bias needs to be focused on more when discussing the model's fidelity in atmospheric ENSO feedback as the too-weak wind response appears in the ENSO's peak and decaying season (boreal late winter) rather than its developing season (summer-autumn). In the late winter, many CMIP6 models fail to reproduce the seasonal southward wind shift albeit it is critical for the rapid decay of strong El Niño events and asymmetry of the ENSO life cycle (McGregor et al., 2012; Stuecker et al., 2013; Abellán & McGregor, 2016). The meridionally confined zonal wind anomalies may also affect the ENSO frequency as narrower wind anomalies are favorable for simulating a shorter period of ENSO (Kirtman, 1997; Capotondi et al., 2006; Lu et al., 2018). Improving the dynamic feedback may provide a more trustful projection of ENSO in a changing climate (Hayashi et al., 2020; Cai et al., 2021; Bayr & Latif, 2022), which needs to be confirmed in further studies.

Acknowledgments

This work was supported by JSPS KAKENHI Grant Number JP21K13993 and MEXT KAKENHI Grant Number JPMXD0722680395.

Open Research

CMIP6 models used can be found in Table S1. The CMIP6 dataset is available at https://esgf-node.llnl.gov/projects/cmip6/, COBE-SST2 at https://climate.mri-jma.go.jp/pub/ocean/cobe-sst2/, GPCP3 at https://measures.gesdisc.eosdis.nasa.gov/data/GPCP/GPCPDAY.3.2/, MSWEP28 at http://www.gloh2o.org/mswep/, CMAP at https://psl.noaa.gov/data/gridded/data.cmap.html, ERA5 at https://doi.org/10.24381/cds.f17050d7 and https://doi.org/10.24381/cds.6860a573, and JRA-55 at https://jra.kishou.go.jp/JRA-55/index_en.html. The data and scripts will be available on the figshare repository.

References

Abellán, E., & McGregor, S. (2016). The role of the southward wind shift in both, the seasonal synchronization and duration of ENSO events. *Climate Dynamics, 47*, 509–527. https://doi.org/10.1007/s00382-015-2853-1

Bayr, T., Dommenget, D., & Latif, M. (2020). Walker circulation controls ENSO atmospheric feedbacks in uncoupled and coupled climate model simulations. *Climate Dynamics, 54*, 2831–2846. https://doi.org/10.1007/s00382-020-05152-2

Bayr, T., & Latif, M. (2022). ENSO atmospheric feedbacks under global warming and their relation to mean-state changes. *Climate Dynamics*. https://doi.org/10.1007/s00382-022-06454-3

Bayr, T., Wengel, C., Latif, M., Dommenget, D., Lübbecke, J., & Park, W. (2019). Error compensation of ENSO atmospheric feedbacks in climate models and its influence on simulated ENSO dynamics. *Climate Dynamics, 53*, 155–172. https://doi.org/10.1007/s00382-018-4575-7

Beck, H. E., Wood, E. F., Pan, M., Fisher, C. K., Miralles, D. G., van Dijk, A. I. J. M., *et al.* (2019). MSWEP v2 global 3-hourly 0.1° precipitation: methodology and quantitative assessment. *Bulletin of the American Meteorological Society*, *100*(3), 473–500. https://doi.org/10.1175/BAMS-D-17-0138.1

Bellenger, H., Guilyardi, E., Leloup, J., Lengaigne, M., & Vialard, J. (2014). ENSO representation in climate models: from CMIP3 to CMIP5. *Climate Dynamics, 42*, 1999–2018. https://doi.org/10.1007/s00382-013-1783-z

Brown, J. R., Brierley, C. M., An, S.-I., Guarino, M.-V., Stevenson, S., Williams, C. J. R., *et al.* (2020). Comparison of past and future simulations of ENSO in CMIP5/PMIP3 and CMIP6/PMIP4 models. *Climate of the Past, 16*, 1777–1805. https://doi.org/10.5194/cp-16-1777-2020

Cai, W., Santoso, A., Collins, M., Dewitte, B., Karamperidou, C., Kug, J.-S., *et al.* (2021). Changing El Niño–Southern Oscillation in a warming climate. *Nature Reviews Earth & Environment, 2*, 628–644. https://doi.org/10.1038/s43017-021-00199-z

Cai, W., Wang, G., Dewitte, B., Wu, L., Santoso, A., Takahashi, K., *et al.* (2018). Increased variability of eastern Pacific El Niño under greenhouse warming. *Nature, 564*, 201–206. https://doi.org/10.1038/s41586-018-0776-9

Capotondi, A., Wittenberg, A., & Masina, S. (2006). Spatial and temporal structure of Tropical Pacific interannual variability in 20th century coupled simulations. *Ocean Modelling, 15*, 274–298. https://doi.org/10.1016/j.ocemod.2006.02.004

Eyring, V., Bony, S., Meehl, G. A., Senior, C. A., Stevens, B., Stouffer, R. J., & Taylor, K. E. (2016). Overview of the Coupled Model Intercomparison Project Phase 6 (CMIP6) experimental design and organization. *Geoscientific Model Development, 9*, 1937–1958. https://doi.org/10.5194/gmd-9-1937-2016

Guilyardi, E., Braconnot, P., Jin, F.-F., Kim, S. T., Kolasinski, M., Li, T., & Musat, I. (2009). Atmosphere feedbacks during ENSO in a coupled GCM with a modified atmospheric convection Scheme. *Journal of Climate*, *22*(21), 5698–5718. https://doi.org/10.1175/2009JCLI2815.1

Guilyardi, E., Capotondi, A., Lengaigne, M., Thual, S., & Wittenberg, A.T. (2020). ENSO modeling: History, progress, and challenges. In M.J. McPhaden, A. Santoso and W. Cai (Eds.), *El Niño Southern Oscillation in a Changing Climate, Geophysical Monograph Series* (Vol. 253, pp. 201–226). Washington, DC: American Geophysical Union. https://doi.org/10.1002/9781119548164.ch9

Hayashi, M., Jin, F.-F., & Stuecker, M. F. (2020). Dynamics for El Niño-La Niña asymmetry constrain equatorial-Pacific warming pattern. *Nature Communications, 11*, 4230. https://doi.org/10.1038/s41467-020-17983-y

Hersbach, H., Bell, B., Berrisford, P., Biavati, G., Horányi, A., Muñoz Sabater, J., *et al.* (2019a). ERA5 monthly averaged data on single levels from 1959 to present, Copernicus Climate Change Service (C3S) Climate Data Store (CDS), Accessed on 15 April 2022. https://doi.org/10.24381/cds.f17050d7

Hersbach, H., Bell, B., Berrisford, P., Biavati, G., Horányi, A., Muñoz Sabater, J., *et al.* (2019b). ERA5 monthly averaged data on pressure levels from 1959 to present, Copernicus Climate Change Service (C3S) Climate Data Store (CDS), Accessed on 9 April 2021. https://doi.org/10.24381/cds.6860a573

Hirahara, S., Ishii, M., & Fukuda, Y. (2014). Centennial-scale sea surface temperature analysis and its uncertainty. *Journal of Climate, 27*, 57–75. https://doi.org/10.1175/JCLI-D-12-00837.1

Huffman, G. J., Behrangi, A., Bolvin, D. T., & Nelkin, E. J. (2022). GPCP version 3.2 daily precipitation data set, Goddard Earth Sciences Data and Information Services Center (GES

DISC), Accessed on 17 October 2022. https://doi.org/10.5067/MEASURES/GPCP/DATA305

Jin, F.-F. (1997). An equatorial ocean recharge paradigm for ENSO. Part I: Conceptual model. *Journal of the Atmospheric Sciences*, *54*(7), 811–829. https://doi.org/10.1175/1520-0469(1997)054<0811:AEORPF>2.0.CO;2

Kim, S. T., Cai, W., Jin, F.-F., & Yu, J.-Y. (2014). ENSO stability in coupled climate models and its association with mean state. *Climate Dynamics, 42*, 3313–3321. https://doi.org/10.1007/s00382-013-1833-6

Kirtman, B. P. (1997). Oceanic Rossby wave dynamics and the ENSO period in a coupled model. *Journal of Climate*, *10*(7), 1690–1704. https://doi.org/10.1175/1520-0442(1997)010<1690:ORWDAT>2.0.CO;2

Kobayashi, S., Ota, Y., Harada, Y., Ebita, A., Moriya, M., Onoda, H., *et al.* (2015). The JRA-55 Reanalysis: General specifications and basic characteristics. *Journal of the Meteorological Sociecty of Japan, 93*, 5–48. https://doi.org/10.2151/jmsj.2015-001

Lee, J., Planton, Y. Y., Gleckler, P. J., Sperber, K. R., Guilyardi, E., Wittenberg, A. T., *et al.* (2021). Robust evaluation of ENSO in climate models: How many ensemble members are needed? *Geophysical Research Letters, 48*, e2021GL095041. https://doi.org/10.1029/2021GL095041

Liu, B., Gan, B., Cai, W., Wu, L., Geng, T., Wang, H., *et al.* (2022). Will increasing climate model resolution be beneficial for ENSO simulation? *Geophysical Research Letters, 49*, e2021GL096932. https://doi.org/10.1029/2021GL096932

Lu, B., Jin, F.-F., & Ren, H.-L. (2018). A coupled dynamic index for ENSO periodicity. *Journal of Climate*, *31*(6), 2361–2376. https://doi.org/10.1175/JCLI-D-17-0466.1

McGregor, S., Cassou, C., Kosaka, Y., & Phillips, A. S. (2022). Projected ENSO teleconnection changes in CMIP6. *Geophysical Research Letters*, 49, e2021GL097511. https://doi.org/10.1029/2021GL097511

McGregor, S., Timmermann, A., Schneider, N., Stuecker, M. F., & England, M. H. (2012). The effect of the South Pacific convergence zone on the termination of El Niño events and the meridional asymmetry of ENSO. *Journal of Climate*, *25*(16), 5566–5586. https://doi.org/10.1175/JCLI-D-11-00332.1

Philander, S. G. (1990). *El Niño, La Niña, and the southern oscillation.* San Diego: CA, Academic Press.

Planton, Y. Y., Guilyardi, E., Wittenberg, A. T., Lee, J., Gleckler, P. J., Bayr, T., *et al.* (2021). Evaluating climate models with the CLIVAR 2020 ENSO metrics package. *Bulletin of the American Meteorological Society*, *102*(2), E193–E217. https://doi.org/10.1175/BAMS-D-19-0337.1

Stuecker, M. F., Timmermann, A., Jin, F.-F., McGregor, S., & Ren, H.-L. (2013). A combination mode of the annual cycle and the El Niño/Southern Oscillation. *Nature Geoscience, 6*, 540–544. https://doi.org/10.1038/ngeo1826

Timmermann, A., An, S.-I., Kug, J.-S., Jin, F.-F., Cai, W., Cobb, K., *et al.* (2018). El Niño-Southern Oscillation complexity. *Nature, 559*, 535–545. https://doi.org/10.1038/s41586-018-0252-6

Wang, X.-Y., Zhu, J., Chang, C.-H., Johnson, N. C., Liu, H., Li, Y., *et al.* (2021). Underestimated responses of Walker circulation to ENSO-related SST anomaly in atmospheric and coupled models. *Geoscience Letters, 8*(17). https://doi.org/10.1186/s40562-021-00186-8

Wengel, C., Lee, S.-S., Stuecker, M. F., Timmermann, A., Chu, J.-E., & Schloesser, F. (2021). Future high-resolution El Niño/Southern Oscillation dynamics. *Nature Climate Change, 11*, 758–765. https://doi.org/10.1038/s41558-021-01132-4

Xie, P., & Arkin, P. A. (1997). Global precipitation: A 17-year monthly analysis based on gauge observations, satellite estimates, and numerical model outputs. *Bulletin of the American Meteorological Society*, *78*(11), 2539–2558. https://doi.org/10.1175/1520-0477(1997)078<2539:GPAYMA>2.0.CO;2

Geophysical Research Letters

Supporting Information for

ENSO feedback biases common to atmosphere-ocean coupled and atmosphere-only simulations of CMIP6 climate models

M. Hayashi[1]

[1]Earth System Division, National Institute for Environmental Studies, Tsukuba, Japan.

Contents of this file

Tables S1 to S2

Introduction

This supplementary information contains the model list used in this study (Table S1) and the linear regression coefficients of various atmospheric anomalies onto the Niño-3.4 sea surface temperature (SST) and equatorial Pacific precipitation anomalies averaged in the observational datasets and the CMIP6 historical and AMIP simulations (Table S2).

Table S1. Model list used in this study.

	Model name	Realization	Unavailable*
1	ACCESS-CM2	r1i1p1f1	
2	ACCESS-ESM1-5	r1i1p1f1	
3	BCC-CSM2-MR	r1i1p1f1	
4	BCC-ESM1	r1i1p1f1	
5	CESM2-WACCM	r1i1p1f1	Us
6	CESM2	r1i1p1f1	Us
7	CMCC-CM2-HR4	r1i1p1f1	
8	CMCC-CM2-SR5	r1i1p1f1	
9	CNRM-CM6-1-HR	r1i1p1f2	
10	CNRM-CM6-1	r1i1p1f2	
11	CNRM-ESM2-1	r1i1p1f2	
12	CanESM5	r1i1p2f1	
13	E3SM-1-0	r1i1p1f1	Us
14	EC-Earth3-AerChem	r1i1p1f1	
15	EC-Earth3-CC	r1i1p1f1	
16	EC-Earth3-Veg	r1i1p1f1	
17	FGOALS-f3-L	r1i1p1f1	
18	FGOALS-g3	r1i1p1f1	Us
19	GFDL-CM4	r1i1p1f1	
20	GISS-E2-1-G	r1i1p1f1	
21	HadGEM3-GC31-LL	r1i1p1f3	
22	INM-CM5-0	r1i1p1f1	
23	IPSL-CM6A-LR	r1i1p1f1	
24	KIOST-ESM	r1i1p1f1	Q, Q_{LH}
25	MIROC-ES2L	r1i1p1f2	
26	MIROC6	r1i1p1f1	
27	MPI-ESM1-2-HR	r1i1p1f1	
28	MPI-ESM1-2-LR	r1i1p1f1	
29	MRI-ESM2-0	r1i1p1f1	
30	NESM3	r1i1p1f1	
31	SAM0-UNICON	r1i1p1f1	Us
32	UKESM1-0-LL	r1i1p1f2	

*The surface zonal wind (Us), net surface heat flux (Q), and surface latent heat flux (Q_{LH}) are not available in some models due to data limitation.

Table S2. Ensemble averaged regression coefficients (observations, historical, AMIP) with units and relative values to observations on average (historical/obs, AMIP/obs).

X variable*	Y variable*	Unit	observations	historical	AMIP	historical/obs	AMIP/obs
Niño-3.4 SST	EqPac P	(mm day^{-1})/°C	1.71	1.28	1.74	75%	102%
Niño-3.4 SST	CPac U	(0.01 N m^{-2})/°C	1.06	0.58	0.90	55%	84%
Niño-3.4 SST	CPac Us	(m s^{-1})/°C	1.00	0.60	0.86	59%	85%
Niño-3.4 SST	CPac U850	(m s^{-1})/°C	2.00	1.33	1.82	66%	91%
Niño-3.4 SST	Niño-3 Ω500	(0.01 Pa s^{-1})/°C	-0.95	-0.58	-0.85	61%	89%
Niño-3.4 SST	Niño-4 Ω500	(0.01 Pa s^{-1})/°C	-2.05	-1.65	-2.38	81%	116%
Niño-3.4 SST	EqPac Q	(W m^{-2})/°C	-15.13	-8.19	-13.59	54%	90%
Niño-3.4 SST	EqPac Q_{SW}	(W m^{-2})/°C	-9.18	-4.87	-8.79	53%	96%
Niño-3.4 SST	EqPac Q_{LW}	(W m^{-2})/°C	0.96	1.11	1.33	115%	138%
Niño-3.4 SST	EqPac Q_{SH}	(W m^{-2})/°C	-1.54	-0.38	-0.90	25%	58%
Niño-3.4 SST	EqPac Q_{LH}	(W m^{-2})/°C	-5.37	-3.96	-5.18	74%	96%
EqPac P	CPac U	(0.01 N m^{-2})/(mm day^{-1})	0.48	0.32	0.38	67%	80%
EqPac P	CPac Us	(m s^{-1})/(mm day^{-1})	0.47	0.36	0.39	76%	83%
EqPac P	CPac U850	(m s^{-1})/(mm day^{-1})	0.95	0.79	0.81	84%	86%
EqPac P	Niño-3 Ω500	(0.01 Pa s^{-1})/(mm day^{-1})	-0.62	-0.48	-0.55	78%	89%
EqPac P	Niño-4 Ω500	(0.01 Pa s^{-1})/(mm day^{-1})	-1.09	-1.28	-1.30	117%	119%
EqPac P	EqPac Q	(W m^{-2})/(mm day^{-1})	-7.32	-6.07	-7.13	83%	97%
EqPac P	EqPac Q_{SW}	(W m^{-2})/(mm day^{-1})	-5.50	-4.55	-5.37	83%	98%
EqPac P	EqPac Q_{LW}	(W m^{-2})/(mm day^{-1})	0.76	1.04	0.92	137%	121%
EqPac P	EqPac Q_{SH}	(W m^{-2})/(mm day^{-1})	-0.75	-0.30	-0.45	40%	60%
EqPac P	EqPac Q_{LH}	(W m^{-2})/(mm day^{-1})	-1.83	-2.20	-2.23	120%	122%

*The Y anomalies are regressed onto the X anomalies. See the main text for the variables and averaged regions.